Ductile Crack Growth Simulations under Mode-I Loading using CTOA Criterion

Sachin Kumar
Department of Mechanical and Industrial Engineering
Indian Institute of Technology Roorkee,
Roorkee, India
sachinsohat1986@gmail.com

I. V. Singh
Department of Mechanical and Industrial Engineering
Indian Institute of Technology Roorkee,
Roorkee, India
ivsingh@gmail.com

B. K. Mishra
Department of Mechanical and Industrial Engineering
Indian Institute of Technology Roorkee,
Roorkee, India
bhanufme@iitr.ac.in

Abstract— **In the present work, extended finite element method (XFEM) has been extended to simulate the large deformation stable crack growth problems using finite strain plasticity. In XFEM, special enrichment functions are employed in the portion of domain where discontinuity and singularity are found whereas the rest of domain is modeled using finite element method. The modeling of large deformation is performed using updated Lagrangian approach. The nonlinear equations obtained as a result of large deformation and nonlinear material behavior, are solved by Newton-Raphson approach. Von-Mises yield criterion has been employed along with isotropic hardening to model finite strain plasticity. The elastic-predictor and plastic-corrector algorithm is employed for stress computation. To verify the proposed CTOA criterion, the results are compared with *J-R* criterion. Two problems i.e. crack growth in compact tension specimen and crack growth in triple point bend specimen are solved under plane stress condition to demonstrate the accuracy and capability of the proposed crack growth criterion.**

Keywords—Stable crack growth; XFEM; large deformation with finite strain plasticity; updated Lagrangian approach; Von-Mises yield criterion; isotropic hardening

I. INTRODUCTION

Generally, fracture analysis may be performed using linear or nonlinear models. Most of the components of the structure are subjected to different type of loading like tension, shear and torsion. It is well known that the component made of ductile material has a stable crack growth before instability. Thus, the instability may occur at a higher load than the crack initiation load in ductile materials. Therefore, elasto-plastic fracture analysis is important to get the full utilization of the material. In the past, stable crack growth in ductile materials under mode-I loading has been studied to develop the efficient techniques for local and global fracture criterion. Some of the criteria to characterize the ductile fracture are crack tip opening angle (CTOA) [1,2], *J*-integral [3,4], tearing modulus [5], and strain energy [6].

Among these criteria, the crack tip opening displacement (CTOD) or crack tip opening angle (CTOA) at a specified distance from the crack tip is the most suited criteria for the modeling of crack growth. The crack tip opening angle (CTOA) is obtained for compact tension specimen [7]. Ma *et al.,* [8] investigated the stable crack growth in aluminum and concluded that the CTOD remains constant under mode-I and mode-II loading. Lam *et al.,* [2] observed that CTOD/CTOA do not remain constant for stable crack growth under plane strain conditions. The initial critical value of CTOD is high due to the crack blunting then it remains constant for further crack growth. Luxmoore *et al.,* [9] experimentally investigated that CTOA remains constant from the onset of stable crack growth in aluminum alloys but have different CTOA values for different crack configuration.

In the past years, a number of numerical methods such as boundary element method [10], finite element method [11], meshfree methods [12] and extended finite element method [13] have been developed for the simulation of fracture problems. In finite element method conformal meshing is required, therefore crack growth modelling is very difficult. To avoid this problem extended finite element method has been widely used in fracture mechanics problems. In XFEM, the effect of discontinues are taken into account by adding some enriched functions into standard finite element approximations, therefore conformal and remeshing is not required.

In this present work, XFEM is applied to simulate the fracture problems. The non-linear equations obtained as a result of large deformation with plasticity are solved by Newton-Raphson technique. Von-Mises yield criterion with isotropic hardening is used to determine the yielding of the material. Constant and varying type of CTOA schemes are determined iteratively to reproduce the experimental results. Several problems are simulated using CTOA/CTOD scheme, to check the effectiveness of the criterion in stable crack growth analysis.

II. MATHEMATICAL FORMULATION

A. Modeling of Large Deformation with Finite Strain Plasticity

Generally, in elasto-plastic analysis two types of non-linearity occurs; (i) material non-linearity and (ii) geometric non-linearity due to large deformation. In this work, geometric nonlinearity is modeled using updated Lagrangian approach. The governing equations for elasto-plasticity with large deformation are given as [14],

$$\nabla.\boldsymbol{\sigma} + \mathbf{b} = \mathbf{0} \;\; in \;\Omega \tag{1}$$

where, $\boldsymbol{\sigma}$ is the Cauchy stress tensor, $\mathbf{b}$ is the body force per unit volume and Ω is the initial domain. In updated Lagrangian approach, "(1)" can be expressed in the variational form as

$$\begin{aligned}\delta\,\boldsymbol{\Psi}(\bar{\mathbf{u}}) = \int_{{}^1\Omega} {}_1^2S_{ij}\,\delta({}_1^2E_{ij})\,d^1\Omega - \int_{{}^1\Omega} b_i\delta u_i\,d^1\Omega \\ - \int_{{}^1\Gamma_t} t_i\delta u_i\,d^1\Gamma = 0\end{aligned} \tag{2}$$

where, ${}_1^2S_{ij}$ are updated second Piola–Kirchhoff stress tensor and ${}_1^2E_{ij}$ are the incremental updated Green-Lagrange strain tensor.

Now using ${}_1^2S_{ij} = {}_1S_{ij} + {}^1\sigma_{ij}$, ${}_1^2E_{ij} = ({}^1E_{ij})_L + ({}^1E_{ij})_{NL}$ "(2)" can be expressed as

$$\begin{aligned}\delta\,\boldsymbol{\Psi}(\bar{\mathbf{u}}) = \int_{{}^1\Omega} {}_1S_{ij}\delta({}_1^2E_{ij})\,d^1\Omega + \int_{{}^1\Omega} {}^1\sigma_{ij}\,\delta({}_1^2E_{ij})\,d^1\Omega \\ - \int_{{}^1\Omega} b_i\delta u_i\,d^1\Omega - \int_{{}^1\Gamma_t} t_i\delta u_i\,d^1\Gamma = 0\end{aligned} \tag{3}$$

$$\begin{aligned}\delta\,\boldsymbol{\Psi}(\bar{\mathbf{u}}) = \int_{{}^1\Omega} {}_1S_{ij}\delta({}_1^2E_{ij})\,d^1\Omega + \int_{{}^1\Omega} {}^1\sigma_{ij}\,\delta({}^1E_{ij})_{NL}\,d^1\Omega \\ + \int_{{}^1\Omega} {}^1\sigma_{ij}\,\delta({}^1E_{ij})_L\,d^1\Omega - \int_{{}^1\Omega} b_i\delta u_i\,d^1\Omega - \int_{{}^1\Gamma_t} t_i\delta u_i\,d^1\Gamma = 0\end{aligned} \tag{4}$$

Since, the incremental displacements u_i are very small in updated Lagrangian approach hence the following approximation can used ${}_1S_{ij} \approx {}_1\mathbf{D}^{ep}({}^1E_{kl})_L$ and $\delta({}_1^2E_{ij}) \approx \delta({}^1E_{ij})_L$. Now, "(3)" takes the form,

$$\begin{aligned}\int_{{}^1\Omega} {}_1\mathbf{D}^{ep}({}^1E_{kl})_L\,\delta({}^1E_{ij})_L\,d^1\Omega \\ + \int_{{}^1\Omega} {}^1\sigma_{ij}\,\delta({}^1E_{ij})_{NL}\,d^1\Omega = \mathbf{R}_{\text{ext}} - \mathbf{R}_{\text{int}}\end{aligned} \tag{5}$$

where, $\mathbf{R}_{\text{int}} = \int_{{}^1\Omega} {}^1\sigma_{ij}\,\delta({}^1E_{ij})_L\,d^1\Omega$ and $\mathbf{R}_{\text{ext}} = \int_{{}^1\Omega} b_i\delta u_i\,d^1\Omega + \int_{{}^1\Gamma_t} t_i\delta u_i\,d^1\Gamma$

Alternatively, the first and second terms of "(5)" can be written as,

$$\begin{aligned}\int_{{}^1\Omega} {}_1\mathbf{D}^{ep}({}^1E_{kl})_L\,\delta({}^1E_{ij})_L\,d^1\Omega = \int_{{}^1\Omega} \left\{\delta({}^1\mathbf{E})_L\right\}^T {}_1\mathbf{D}^{ep}({}^1\mathbf{E})_L\,d^1\Omega \\ = \int_{{}^1\Omega} \delta\bar{\mathbf{u}}^T\mathbf{B}^T{}_1\mathbf{D}^{ep}\mathbf{B}\bar{\mathbf{u}}\,d^1\Omega = \delta\bar{\mathbf{u}}^T\mathbf{K}^{\text{mat}}\bar{\mathbf{u}}\end{aligned} \tag{6}$$

$$\begin{aligned}\int_{{}^1\Omega} {}^1\sigma_{ij}\,\delta({}^1E_{ij})_{NL}\,d^1\Omega = \int_{{}^1\Omega} \left\{\delta({}^1\mathbf{E})_{NL}\right\}^T {}^1\sigma_{ij}\,d^1\Omega \\ = \int_{{}^1\Omega} \delta\bar{\mathbf{u}}^T\,\mathbf{G}^T\mathbf{M}_{\boldsymbol{\sigma}}\,\mathbf{G}\bar{\mathbf{u}}\,d^1\Omega = \delta\bar{\mathbf{u}}^T\,\mathbf{K}^{geo}\,\bar{\mathbf{u}}\end{aligned} \tag{7}$$

where, $\mathbf{K}^{\text{mat}} = \int_\Omega \mathbf{B}^T\mathbf{D}^{ep}\mathbf{B}\,d\Omega$, $\mathbf{K}^{\text{geo}} = \int_\Omega \mathbf{G}^T\mathbf{M}_{\boldsymbol{\sigma}}\mathbf{G}\,d\Omega$

Using "(6)" and "(7)" "(5)"can be further written as,

$$\delta\bar{\mathbf{u}}^T\,\mathbf{K}^{\text{mat}}\,\bar{\mathbf{u}} + \delta\bar{\mathbf{u}}^T\,\mathbf{K}^{geo}\,\bar{\mathbf{u}} = \mathbf{R}_{\text{ext}} - \mathbf{R}_{\text{int}} \tag{8}$$

Using $\mathbf{R}_{\text{ext}} = \delta\bar{\mathbf{u}}^T\,\mathbf{f}_{\text{ext}}$ and $\mathbf{R}_{\text{int}} = \delta\bar{\mathbf{u}}^T\,\mathbf{f}_{\text{int}}$, "(8)" can be modified as,

$$\delta\bar{\mathbf{u}}^T\,(\mathbf{K}^{\text{mat}} + \mathbf{K}^{geo})\,\bar{\mathbf{u}} = \delta\bar{\mathbf{u}}^T\,(\mathbf{f}_{\text{ext}} - \mathbf{f}_{\text{int}}) \tag{9}$$

where, external force ($\mathbf{f}_{\text{ext}}$) and internal force ($\mathbf{f}_{\text{int}}$) can be defined as,

$$\mathbf{f}_{\text{ext}} = \int_{{}^1\Omega} \mathbf{b}^1 d^1\Omega + \int_{{}^1\Omega} \mathbf{t}^1 d^1\Omega \tag{10}$$

$$\mathbf{f}_{\text{int}} = \int_{{}^1\Omega} \mathbf{B}^{T\,1}\boldsymbol{\sigma}\,d^1\Omega \tag{11}$$

From "(10)" finally we get,

$$(\mathbf{K}^{\text{mat}} + \mathbf{K}^{geo})\,\bar{\mathbf{u}} = \mathbf{f}_{\text{ext}} - \mathbf{f}_{\text{int}} \tag{12}$$

where, $\mathbf{K}^{\mathbf{mat}}$ and $\mathbf{K}^{\mathbf{geo}}$ are the material tangent stiffness matrix and geometric stiffness matrix respectively; $\mathbf{M}_{\boldsymbol{\sigma}}$ is the matrix of Cauchy stress components; and $\mathbf{B}$, $\mathbf{G}$ are Cartesian shape function derivatives matrix.

Von-Mises yield criterion with isotropic strain hardening is used to obtain the stress level at which plasticity begins. During any increment of stress, the change of strain are assumed to be divisible into elastic and plastic components [15],

$$d\varepsilon_{ij} = (d\varepsilon_{ij})^e + (d\varepsilon_{ij})^p \tag{13}$$

After decomposing the stresses into deviatoric and hydrostatic components and assuming the associated theory of plasticity, "(13)" can be written as,

$$d\varepsilon_{ij} = \frac{d\sigma'_{ij}}{2G} + \frac{(1-2\nu)}{E}\delta_{ij}d\sigma_{kk} + d\lambda\frac{\partial f}{\partial\sigma_{ij}} \tag{14}$$

where, f is the yield function and $d\lambda$ is a proportionality constant termed as the plastic multiplier. Now the elasto-plastic incremental stress-strain relation is obtained as,

$$d\boldsymbol{\sigma} = \mathbf{D}_{ep}d\boldsymbol{\varepsilon} \tag{15}$$

where, $\mathbf{D}_{ep} = \mathbf{D} - \dfrac{\mathbf{d}_D\mathbf{d}_D^T}{A + \mathbf{d}_D^T\mathbf{a}}$, $\mathbf{d}_D^T = \mathbf{a}^T\mathbf{D}$, $\mathbf{a}^T = \dfrac{\partial F}{\partial\boldsymbol{\sigma}}$,

and $A = -\dfrac{1}{d\lambda}\dfrac{\partial F}{\partial k}dk$

As stated above, the associated theory [16] of plasticity, $f \equiv Q$, yield function and potential function are identical, thus the elasto-plastic constitutive matrix $\mathbf{D}_{ep}$ becomes symmetric.

B. Displacement Approximation for Crack

In XFEM, Discontinuities are modeled by locally adding some enrichment terms into the standard finite element approximation. A shifted enrichment is used to recover the Kronecker delta property in the enriched elements. In two-dimension, at a particular node of interest $\mathbf{x}_i$, the displacement approximation can be written as [13,17],

$$\mathbf{u}^h(\mathbf{x}) = \sum_{i=1}^{n} N_i(\mathbf{x})\bar{\mathbf{u}}_i + \sum_{i=1}^{n} N_i(\mathbf{x})\underbrace{[H(\mathbf{x}) - H(\mathbf{x}_i)]\mathbf{a}_i}_{i \in n_r} + \sum_{i=1}^{n} N_i(\mathbf{x})\underbrace{\sum_{\alpha=1}^{4}[\beta_\alpha(\mathbf{x}) - \beta_\alpha(\mathbf{x}_i)]\mathbf{b}_i^\alpha}_{i \in n_A} \quad (16)$$

where, $\bar{\mathbf{u}}_i$ is a nodal displacement vector associated with the continuous part of the FE solution, $\mathbf{a}_i$ is the nodal enriched degree of freedom associated with discontinuous Heaviside function $H(\mathbf{x})$, and $\mathbf{b}_i^\alpha$ is the nodal enriched degree of freedom vector associated with crack tip enrichment ($\beta_\alpha(\mathbf{x})$). $\beta_\alpha(\mathbf{x})$ is the asymptotic crack tip enrichment functions, n is the set of all nodes in the mesh, n_r is the set of nodes belonging to those elements which are completely cut by the crack and n_A is the set of nodes belonging to those elements which are partially cut by the crack.

C. Discontinuous Enrichment for Crack Face

The discontinuity in the displacement due to crack is modeled by a generalized Heaviside function $H(\mathbf{x})$ and can be defined as:

$$H(\mathbf{x}) = \begin{cases} 1 & if \;\; \chi(\mathbf{x}) \geq 0 \\ -1 & otherwise \end{cases} \quad (17)$$

where, $\chi(\mathbf{x})$ is the level set function.

D. Asymptotic Enrichment for Crack Tip

In this enrichment, four functions are used to model the radial as well as the angular behavior of asymptotic crack-tip stress fields. These functions are given as [18],

$$\beta_\alpha(\mathbf{x}) = \{\beta_1, \;\beta_2, \;\beta_3, \;\beta_4\} = r^k\left[\cos\frac{\theta}{2}, \;\sin\frac{\theta}{2}, \;\cos\frac{\theta}{2}\sin\theta, \;\sin\frac{\theta}{2}\sin\theta\right] \quad (18)$$

In the above expression, r and θ are the local coordinates of the crack tip. For LEFM enrichment functions $k = 0.5$, and for EPFM enrichment functions $k = \left(\frac{1}{1+n}\right)$, where n is the hardening exponent that depends on material.

The elemental matrices, $\bar{\mathbf{K}}_T$ and $\mathbf{f}$ are obtained by substituting the approximation function, defined in "(16)" into "(10)" and "(12)"

$$\bar{\mathbf{K}}_{Tij} = \begin{bmatrix} \mathbf{K}_{ij}^{uu} & \mathbf{K}_{ij}^{ua} & \mathbf{K}_{ij}^{ub} \\ \mathbf{K}_{ij}^{au} & \mathbf{K}_{ij}^{aa} & \mathbf{K}_{ij}^{ab} \\ \mathbf{K}_{ij}^{bu} & \mathbf{K}_{ij}^{ba} & \mathbf{K}_{ij}^{bb} \end{bmatrix} \quad (19)$$

$$\mathbf{f}^h = \{\mathbf{f}_i^{\mathbf{u}} \quad \mathbf{f}_i^{\mathbf{a}} \quad \mathbf{f}_i^{\mathbf{b1}} \quad \mathbf{f}_i^{\mathbf{b2}} \quad \mathbf{f}_i^{\mathbf{b3}} \quad \mathbf{f}_i^{\mathbf{b4}}\}^T \quad (20)$$

The sub-matrices and vectors that appear in the foregoing equations are given as

$$\bar{\mathbf{K}}_{ij}^{rs} = \int_{\Omega^e} (\mathrm{B}_i^r)^T \mathbf{D}^{ep}\, \mathrm{B}_j^s \, hd\Omega + \int_{\Omega^e} (\mathbf{G}_i^r)^T \mathbf{M}_\sigma \mathbf{G}_j^s \, hd\Omega \quad (21)$$

where, $r, s = u, a, b$

$$\mathbf{f}_i^u = \int_{\Omega^e} N_i \mathbf{b}\, d\Omega + \int_{\Gamma_t} N_i \bar{\mathbf{t}}\, d\Gamma \quad (22)$$

$$\mathbf{f}_i^a = \int_{\Omega^e} N_i\,(H(\mathbf{x}) - H(\mathbf{x}_i))\,\mathbf{b}\, d\Omega + \int_{\Gamma_t} N_i\,(H(\mathbf{x}) - H(\mathbf{x}_i))\,\bar{\mathbf{t}} d\Gamma \quad (23)$$

$$\mathbf{f}_i^{b\alpha} = \int_{\Omega^e} N_i \beta_\alpha((\mathbf{x}) - (\mathbf{x}_i))\mathbf{b} d\Omega + \int_{\Gamma_t} N_i(\beta_\alpha(\mathbf{x}) - (\mathbf{x}_i))\bar{\mathbf{t}} d\Gamma \quad (24)$$

where, $\alpha = 1,2,3,4$ and N_i are finite element shape function, $\mathbf{B}_i^u$, $\mathbf{B}_i^a$, $\mathbf{B}_i^b$ and $\mathbf{B}_i^{b\alpha}$ are the matrices of shape function derivatives and $\mathbf{G}_i^u$, $\mathbf{G}_i^a$, $\mathbf{G}_i^b$ and $\mathbf{G}_i^{b\alpha}$ are the matrices of Cartesian shape function derivatives.

III. NUMERICAL SIMULATION

In this section, stable crack growth in compact tension specimen is simulated under plane stress condition. The nonlinear material behavior is modeled using Ramberg-Osgood material model given as [18],

$$\frac{\varepsilon}{\varepsilon_o} = \frac{\sigma}{\sigma_Y^0} + \bar{\alpha}\left(\frac{\sigma}{\sigma_Y^0}\right)^{\bar{n}} \quad (25)$$

where is σ_Y^o the initial yield stress, ε_o is the strain and are $\bar{n}$ and $\bar{\alpha}$ the model parameters usually taken from the true stress and true strain curve.

A. Geometry of CT Specimen with dimensions

The full geometry of a CT specimen is shown in "Fig. 1". A typical discretization of CT specimen with uniform mesh using four node quadrilateral elements is given in "Fig. 2". In the meshed geometry, star, hexagon and square are used to represent the split, tip and fictitious nodes respectively. Fictitious nodes are used to keep the same number of unknowns when the crack grows. The crack mouth opening displacement (CMOD) is measured at the black dotted nodes, just above and below the crack. The displacement is applied at the nodes circled in red. The green color elements are modeled as stiff elements to avoid local deformation.

1) 3.1.1 Crack Growth in Compact Tension Specimen using CTOD/CTOA Criterion

The CT specimen dimensions, $L = 120\,\text{mm}$, $W = 100\,\text{mm}$, $B = 8\,\text{mm}$, $a/W = 0.43$ are shown in Fig. 1. The material properties corresponding to AISI 4340 steel reported by [19] are: Young modulus, $E = 198\,\text{GPa}$, yield strength, $\sigma_Y^o = 487\,\text{MPa}$ and Poisson's ratio, $\mu = 0.30$. The Ramberg-Osgood dimensionless parameters ($\bar{n} = 9.489$ and $\bar{\alpha} = 0.845$) are derived from the true stress and true strain diagram of this material. A uniform mesh consisting of 63 equally distributed nodes in x-direction and 50 equally distributed nodes in y-direction is used for the simulation. Crack tip opening or crack tip angle value is used as crack growth criterion for this problem. As the criterion gets satisfied, the crack length is increased by a specified amount (0.81 mm per step). Two different types of CTOD/CTOA schemes are used: first constant

CTOD/CTOA scheme and second varying CTOD/CTOA scheme. CTOD is measured 0.5 mm behind the crack tip as shown in "Fig. 3", and CTOA is determined from CTOD as CTOA = CTOD/0.50 radian.

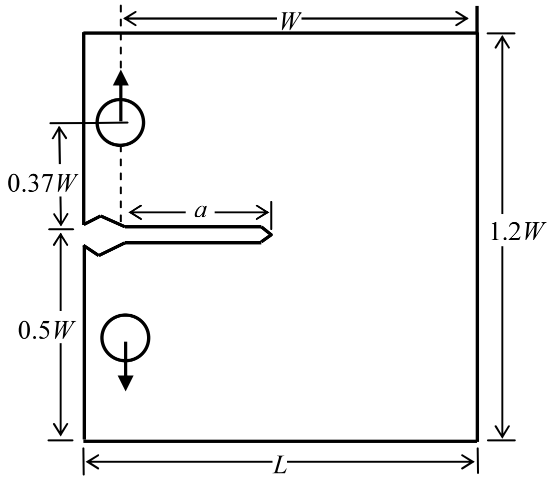

Fig. 1. Compact tension (CT) specimen with dimensions

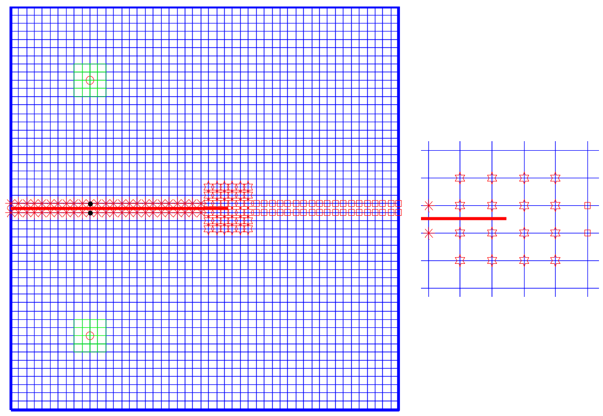

Fig. 2. Typical discretization of the CT Specimen

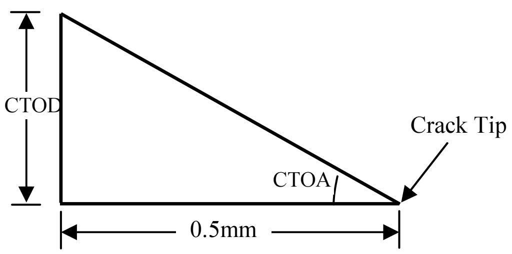

Fig. 3. CTOD/CTOA criterion

2) Constant CTOD/CTOA scheme

In this scheme, CTOD/CTOA remains constant throughout the stable crack growth analysis. The different critical values of CTOD/CTOA are used in numerical experimentation. For selected assumed values of CTOD/CTOA, the load versus CMOD diagrams are predicted and compared with experimental results as shown in "Fig. 4". The crack initiation load P_i and maximum load P_{max} are compared in Table 1 for different trial values of CTOD/CTOA. From these results, it is observed that as the CTOA value increases, the error in crack initiation load decreases but the same in maximum load increases. A significant difference is found between experimental and predicted CMOD value corresponding to the maximum load. For CTOA = 0.0310 radian, a difference of 0.14% is found between experimental and predicted crack initiation load whereas a difference of 8.18% is noticed in maximum load. A similar observation in maximum load is found by [2, 20]. By using CTOA = 0.0280 radian and 0.0290 radian, the error in the maximum load decreases further but the error in predicting crack initiation load increases. The variation of load and *J*-integral for different constant CTOD/CTOA values is shown in "Fig.5".

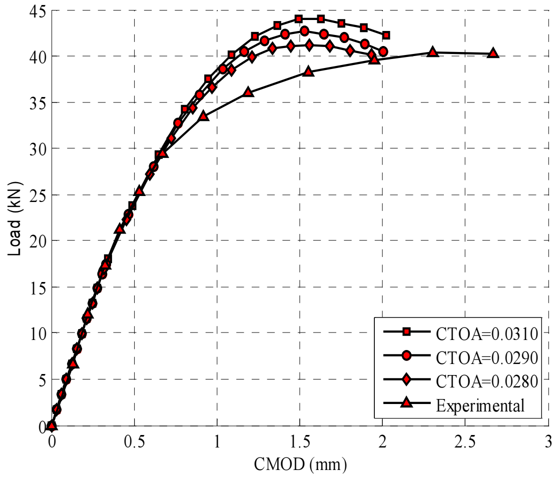

Fig. 4. Comparison of experimental and XFEM load versus CMOD plots for different constant CTOA values

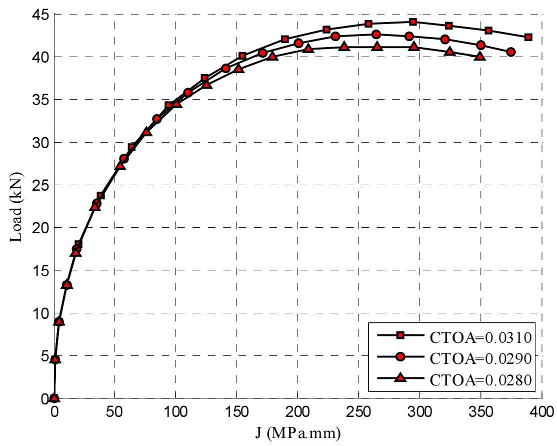

Fig. 5. Load versus *J*-integral plots for different CTOA values

In the "Fig. 5", different critical CTOD/CTOA values are used for the simulation. For the some initial load steps, the value of CTOD/CTOA increases and obtain the critical CTOD/CTOA value, hence extension in crack length. This crack extension decreases the CTOD/CTOA value for further crack growth keeping the critical CTOD/CTOA constant. Initially, the different critical CTOD/CTOA values show a very good match between load and *J*-integral values but the difference increases with the crack extension. Load versus Δa variation for different constant CTOA values are given in "Fig. 6". The maximum load value increases with the increase in CTOD/CTOA values. The stable crack growth is found same for all the cases. A stress contour plot of σ_{yy} for (constant CTOA = 0.0310 radian) corresponding to the final stage loading is shown in "Fig. 7". The stress level is plotted in MPa.

TABLE I. COMPARISON OF PREDICTED LOAD AND CMOD BASED ON DIFFERENT TRIAL VALUES OF CTOD/CTOA CRITERION WITH EXPERIMENTAL VALUES FOR $a/W = 0.43$

CTOA (radian)	P_i			P_{max}		
	Exp.	*XFEM*	*% error*	*Exp.*	*XFEM*	*% error*
0.0280	18.00	16.97	5.72	40.40	41.11	1.73
0.0290	18.00	17.50	2.76	40.40	42.76	5.53
0.0310	18.00	18.03	0.14	40.40	44.00	8.18

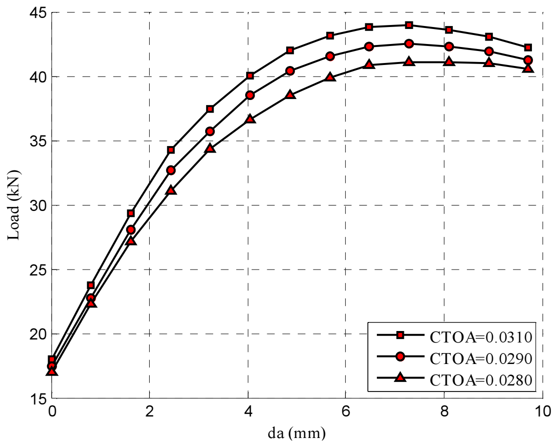

Fig. 6. Load versus Δa plots for different CTOA values

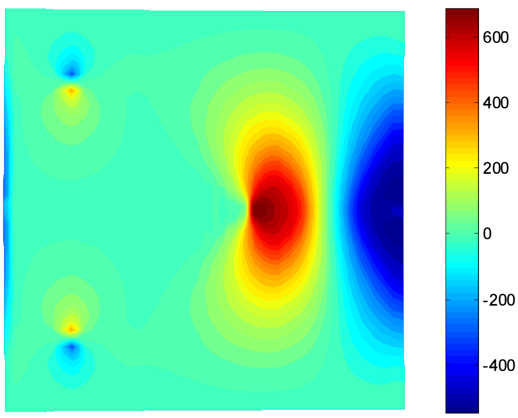

Fig. 7. Stress contour plot (σ_{yy}) for CT Specimen

3) Varying CTOD/CTOA scheme

Two more schemes of varying CTOD/CTOA with crack extension are further considered as shown in "Fig. 8". The initial CTOD/CTOA values for both the schemes are 0.0155mm/0.0310 radian. In the first scheme, the value of CTOA decreases initially and then increases and finally becomes constant. In the second scheme, the CTOA values decreases and then remains constant. The results obtained by these two approaches are compared with experimental data as shown in "Fig. 9" and Table 2. From these results, an overall improvement is observed in the predicted load versus CMOD plot. From the table, it is observed that the scheme-1 has smaller error in both the maximum load and CMOD.

TABLE II. COMPARISON OF PREDICTED LOADS AND CMOD BASED ON DIFFERENT SCHEMES WITH EXPERIMENTAL VALUES FOR $a/W = 0.43$

Scheme No.	P_i			P_{max}		
	Exp.	*XFEM*	*% error*	*Exp.*	*XFEM*	*% error*
Scheme-1	18.00	18.025	0.14	40.40	40.933	1.32
Scheme-2	18.00	18.025	0.14	40.40	38.815	3.92

From the results predicted using different schemes, it is clear that the initial stages of crack extension are associated with the decreasing CTOD/CTOA values. This type of variation in CTOD/CTOA values has been used by other investigators [1,2].

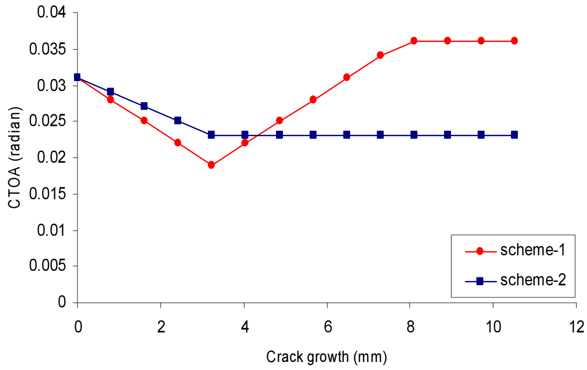

Fig.8. Two schemes of varying CTOA with crack growth

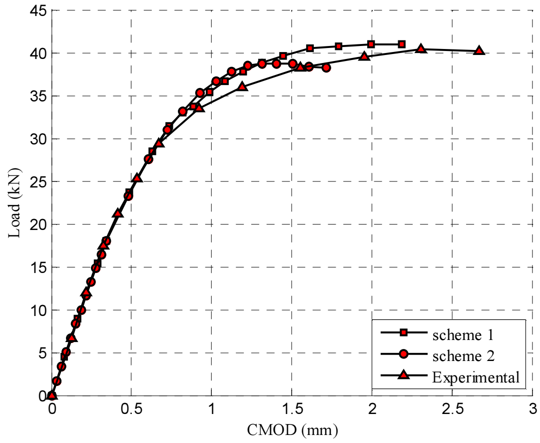

Fig. 9. Comparison of experimental and predicted load-CMOD diagrams based on different schemes

B. Crack Growth in Triple Point Bend Specimen using J-R Curve

The geometric dimensions of triple point bend (TPB) specimen are taken as $W = 50.8$ mm , $B = 25.04$ mm , $L = 362$ mm , $a = 31.90$ mm as shown in "Fig. 10". The material used is HY100 steel, whose properties are taken from the literature [4] as follows: Young modulus $E = 200\,\text{GPa}$, yield strength $\sigma_Y^0 = 710\,\text{MPa}$ and Poisson's ratio $\mu = 0.30$. The Ramberg-Osgood material model ($\bar{n} = 15.5$ and $\bar{\alpha} = 0.85$) defined in "(25)" is used to model the nonlinear behavior of the material. A uniform mesh consisting of 80 equally spaced nodes in x-direction and 40 equally spaced nodes in y-direction is used for the simulation. A crack increment of 0.20 mm per instance is taken for the simulations. The value of J_{cr} is 180 MPa-mm.

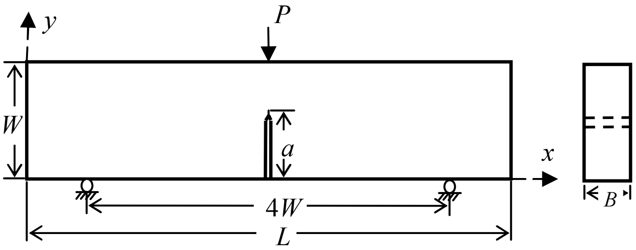

Fig. 10. Triple Point Bend specimen with dimensions

The stable crack growth analysis in TPB specimen is carried out using bilinear variation of CTOA with the crack extension. Different CTOA values are used for crack extension in numerical simulation. CTOA = 0.145 radian for crack initiation is found to be most suitable. After crack initiation, critical value of CTOA decreases to 0.120 radian, and then it remains constant during further crack extension. The load versus CMOD values obtained using CTOA and *J-R* criteria are shown in "Fig. 11". From the results presented in "Fig. 11", it is observed that the results reproduced by above assumed critical CTOA are found in good agreement with those obtained using *J-R* criterion. A similar CTOA variation has been assumed earlier by other researchers [2, 21].

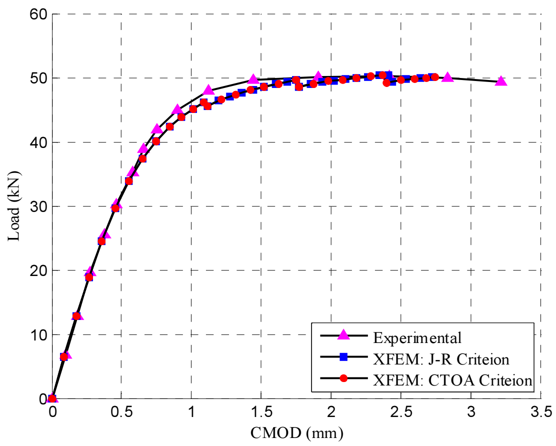

Fig. 11. Comparison of experimental and XFEM results using different criterions for TPB specimen

The *J-R* and above assumed CTOA criteria are further used for compact tension specimen. The dimensions of the CT specimen are used as reported in [22] and the material properties are taken from the paper [4]. A comparison of load with CMOD using different criteria is shown in "Fig.12". The load–CMOD plots are found in excellent agreement. Hence, it can be concluded that the critical CTOA can be used as a fracture criterion for crack growth in different types of specimens.

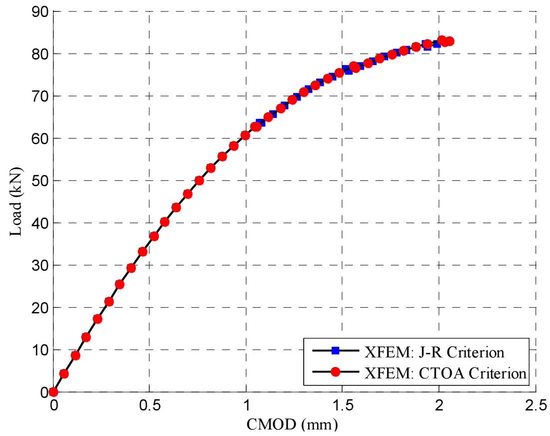

Fig. 12. Comparison of CT specimen load versus CMOD plot using different criterions

IV. Conclusions

In the present study, stable crack growth in CT and TPB specimens has been modeled and simulated by XFEM under plane stress condition. Scope of CTOD/CTOA criterion for the stable crack growth has been numerically investigated. Various constant critical values of CTOD/CTOA are assumed, and the load versus CMOD plots was obtained. A good agreement in crack initiation load was observed but the maximum load was underestimated. Later, two schemes with varying critical CTOD/CTOA are used. These schemes predict the crack initiation and maximum loads close to the experimental values.

Stable crack propagation in triple point bend specimen has also been modeled using *J-R* approach. Again, a good match with experimental results has been observed. A variable critical CTOA scheme with "initially decreasing and later constant" type CTOA is found to be in good agreement with the experimental results. The *J-R* curve and the critical CTOA values obtained from the simulation of triple point bend specimen are further used to model a CT specimen, and the load–CMOD plots obtained by these two criteria showed an excellent agreement in the results. On the basis of present simulations, it can be concluded that CTOD/CTOA is an effective criterion for modeling stable crack growth in ductile materials. This work can be further extended to simulate stable crack problems under mixed mode loading.

References

[1] J.C. Newman Jr., M.A. James and U. Zerbst, "A review of the CTOA/CTOD fracture criterion," *Engineering Fracture Mechanics*, vol. 70, pp. 371–385, 2003.

[2] P.S. Lam, Y. Kim and Y.J. Chao, "The non-constant CTOD/CTOA in stable crack extension under plane-strain conditions," *Engineering Fracture Mechanics*, vol. 73, pp. 1070–1085, 2006.

[3] J.R. Rice, "A path independent integral and the approximate analysis of strain concentration by notches and cracks," Journal of Applied Mechanics, vol. 35, pp. 379–386, 1968.

[4] G.P. Zhu, G.M.C. Lee and A.A. Mufti, "An experimental and computational investigation of crack initiation and stable crack growth of ductile materials," Finite Elements in Analysis and Design, vol. 13, pp. 259–269, 1993.

[5] P.C. Paris, H. Tada, Z. Zahoor and H. Ernst, "Instability of the tearing mode of elastic plastic crack growth," *In: Elastic–Plastic Fracture, ASTM STP 668*, pp. 5–36, 1979.

[6] A.P. Kfouri and K.J. Miller, "Crack Separation Energy Rates in Elastic-Plastic Fracture Mechanics," *Proceedings of the Institution of Mechanical Engineers*, vol. 190, pp. 571–584, 1976.

[7] S. Xu, N. Petri and W.R. Tyson, "Evaluation of CTOA from load-line displacement for C(T) specimen," Engineering Fracture Mechanics, vol. 76, pp. 2126-2134, 2009.

[8] L. Ma, P.W. Lam, M.T. Kokaly and A.S. Kobayashi, "CTOA of a stable crack in a thin aluminum fracture specimen," *Engineering Fracture Mechanics,* vol. 70, pp. 427-442, 2003.

[9] A. Luxmoore, M.F. Light and W.T. Evans, "A comparison of energy release rates, the J-integral and crack tip displacements," *International Journal of Fracture*, vol. 13, pp. 257-259, 1977.

[10] A.A. Portela, M. Aliabadi and D. Rooke, "The dual boundary element method: effective implementation for crack problems," International Journal for Numerical Methods in Engineering, vol. 33, pp. 1269–1287, 1991.

[11] S. Cheung and A. R. Luxmoore, "A finite element analysis of stable crack growth in an aluminium alloy," *Engineering Fracture Mechanics*, vol. 70, pp. 1153–1169, 2003.

[12] T. Belytschko, L. Gu and Y.Y. Lu, "Fracture and crack growth by element-free Galerkin methods," *Modelling and Simulation in Material Science and Engineering*, vol. 2, pp. 519–534, 1994.

[13] T. Belytschko and T. Black, "Elastic crack growth in finite elements with minimal remeshing," *International Journal for Numerical Methods in Engineering*, vol. 45, pp. 601–620, 1999.

[14] J.N. Reddy, "An introduction to nonlinear finite element analysis," Oxford University Press, pp. 327–353, 2009.

[15] E. Hinton and D.R.J. Owen, "Finite Element in Plasticity," *Pineridge Press Limited*, pp. 215-265, 1980.

[16] D. R. Bland, "The associated flow rule of plasticity," *Journal of Mechanics and Physics of Solids*, vol. 6, pp. 71–78, 1957.

[17] I.V. Singh, B.K. Mishra, S. Bhattacharya and R.U. Patil, "The numerical simulation of fatigue crack growth using extended finite element method," International Journal of Fatigue, vol. 36, pp. 109–119, 2012.

[18] B.N. Rao and S. Rahman, "An enriched meshless method for non-linear fracture mechanics," International Journal for Numerical Methods in Engineering, vol. 59, pp. 197–223, 2004.

[19] A.H.I. Mourad, M.J. Alghafri, O.A.A. Zeid and S.K. Maiti, "Experimental investigation on ductile stable crack growth emanating from wire-cut notch in AISI 4340 steel," Nuclear Engineering and Design, vol. 235, pp. 637-647, 2005.

[20] S.K. Maiti, G.K. Kishore and A.H.I. Mourad, "Bilinear CTOD/CTOA scheme for characterisation of large range mode I and mixed mode stable crack growth through AISI 4340 steel," *Nuclear Engineering and Design*, vol. 238, pp. 3175–3185, 2008.

[21] S. Mahmoud and K. Lease, "The effect of specimen thickness on the experimental characterization of critical CTOA in 2024-T351 aluminum alloy, *Engineering Fracture Mechanics*, vol. 70, pp. 443–456, 2003.

[22] D.K. Mahanty and S.K. Maiti, "Experimental and finite element studies on mode-I and mixed mode (I and II) stable crack growth-I. Experimental," *Engineering Fracture Mechanic*s, vol. 37, pp. 1237–1250, 1990.